

# Formulation and interpretation of optimal braking and steering patterns towards autonomous safety-critical manoeuvres

Victor Fors, Björn Olofsson & Lars Nielsen

To cite this article: Victor Fors, Björn Olofsson & Lars Nielsen (2019) Formulation and interpretation of optimal braking and steering patterns towards autonomous safety-critical manoeuvres, *Vehicle System Dynamics*, 57:8, 1206-1223, DOI: [10.1080/00423114.2018.1549331](https://doi.org/10.1080/00423114.2018.1549331)

To link to this article: <https://doi.org/10.1080/00423114.2018.1549331>



© 2018 The Author(s). Published by Informa UK Limited, trading as Taylor & Francis Group



Published online: 25 Nov 2018.



Submit your article to this journal [↗](#)



Article views: 1282



View related articles [↗](#)





View Crossmark data [↗](#)



Citing articles: 3 View citing articles [↗](#)

# Formulation and interpretation of optimal braking and steering patterns towards autonomous safety-critical manoeuvres

Victor Fors , Björn Olofsson  and Lars Nielsen

Division of Vehicular Systems, Department of Electrical Engineering, Linköping University, Linköping, Sweden

## ABSTRACT

Stability control of a vehicle in autonomous safety-critical at-the-limit manoeuvres is analysed from the perspective of lane keeping or lane changing, rather than that of yaw control as in traditional ESC systems. An optimal control formulation is developed, where the optimisation criterion is a linear combination of the initial and final velocity of the manoeuvre. Varying the interpolation parameter in this formulation turns out to result in an interesting family of optimal braking and steering patterns in stabilising manoeuvres. The two different strategies of optimal lane-keeping control and optimal yaw control are shown to be embedded in the formulation and result from the boundary values of the parameter. The results provide new insights and have the potential to be used for future safety systems that adapt the level of braking to the situation at hand, which is demonstrated through examples of how to exploit the results.

## ARTICLE HISTORY


Received 7 December 2017  
Revised 5 November 2018  
Accepted 6 November 2018

## KEYWORDS

Vehicle stability; yaw control; lane keeping; lane change; avoidance manoeuvre; at-the-limit

## 1. Introduction

Active-safety and driver-assistance systems are fundamental components in modern passenger cars as well as trucks. Common examples include the anti-lock braking system (ABS) and the electronic stability control (ESC) system [1]. Another opportunity to reduce the number of accidents and the severity of the associated injuries, is the strong trend towards autonomy of vehicles with the ultimate goal of completely autonomous cars. On the path to fully autonomous vehicles, semi-autonomous features and active-safety systems, which are complementary to each other, are appearing on the market. Motivated both by safety and by autonomy, there has recently been an increased interest in finding alternatives to traditional ESC systems, such that the dynamics of the vehicle is fully exploited. In particular, it is desirable to utilise the maximum available tyre forces in combination with optimal steering inputs in safety-critical manoeuvres where the vehicle performs at the limit.

**CONTACT** Victor Fors  [victor.fors@liu.se](mailto:victor.fors@liu.se)

## 1.1. Background

In [2], an analysis of the possible benefits of increased situation awareness and autonomous optimisation-based lane-keeping stability-control systems for vehicles was performed. In that paper, the focus was to quantify the maximum initial velocity that could be handled in a left-hand turn, in the two cases of an optimal active yaw-control system and of an optimal lane-keeping control system. Both cases included optimal steering angles, assuming complete autonomy without human intervention, and the evaluation was performed using several different scenarios that differed in terms of turn geometry and road conditions. In [3], different actuator configurations of a vehicle were examined by quantifying the maximum initial velocity that could be handled, using similar scenarios as those considered in this paper. Optimal manoeuvres in a hairpin turn for different surfaces were computed using numerical dynamic optimisation in [4]. Torque vectoring for minimum-time cornering was examined in [5] by using optimal steering inputs. In [6], a comparison of the optimal manoeuvres in a turn with the criteria of minimum time and maximum exit velocity, respectively, was presented using an optimal-control approach. Investigation of the mitigation of secondary collisions after impact was performed using optimal-control methods in [7]. A subsequent control design was presented in [8] based on the findings from optimal control. In [9], an accident-avoidance framework was presented that takes advantage of road preview information to intervene earlier than traditional ESC systems, which included an MPC approach for simultaneous braking and steering. Research related to the subject matter of the current paper was also presented in [10], where a control law referred to as the parabolic path reference strategy (PPR) was proposed. The PPR strategy was shown to result in good performance compared to conventional yaw control, when evaluated in a semi-autonomous, critical left-hand turn scenario, employing a double-track vehicle model. The PPR strategy was integrated and developed into a complete control design for roads comprising more complex geometries in [11]; that paper also proposed a strategy to track desired yaw moments during the manoeuvres.

## 1.2. A family of braking and steering patterns – motivation and contributions

In this paper, we present an analysis that extends the results in [2], is complementary to [10,11], and continues the investigation started in [12]. We investigate the optimal braking and steering patterns in completely autonomous (in the sense that no driver or driver-model is assumed) safety-critical manoeuvres in the relevant scenarios of optimal braking and steering in a left-hand turn, in a double lane-change, and in an avoidance situation, which are all introduced in Section 3. Key contributions in this paper are the results stemming from the formulation of the optimisation criterion (4a), which is a linear combination of the initial velocity and final velocity. The intuition behind this formulation is that maximising the initial velocity means that all-wheel braking is typically performed to reduce the velocity so as to stay in lane, and the resulting control strategy is a vehicle behaviour that is called optimal lane keeping. On the other hand, if the initial velocity is lower than the maximum possible to handle in a given situation, it may be advantageous to not apply unnecessarily high braking torques, and this can loosely be formulated as maximising the final velocity. This criterion enables the study of how the optimal use of the actuators changes as less braking is encouraged.

The benefits of an optimal lane-keeping strategy are clear, both in terms of the maximum possible initial velocity, while still staying on the road, and the velocity reduction obtained with all-wheel braking. It is well known that the risk of injury or even fatalities in an accident increases severely with the velocity in an impact. Thus, applying all-wheel braking immediately when detecting a critical manoeuvring situation is beneficial also in the cases where the tyre friction is not sufficient to completely prevent an accident, since the velocity is decreased before an inevitable crash. The motivation behind the weighted optimisation criterion is to gain insights into the trade-off between the all-wheel braking strategies observed in [2] when using an optimisation criterion to maximise the initial velocity, and less braking-intensive strategies. Less braking-intensive strategies provide insights into how the braking forces are utilised to keep the vehicle on the road, apart from decreasing its velocity. An interesting question is if the traditional yaw control and ESC strategies will emerge in less braking-intensive, but still optimal, autonomous strategies. These results have the possibility to be applicable for a wider range of scenarios than those examined, and for vehicles with other characteristics than the one in this paper.

Further, the optimisation criterion itself can be of interest for formulating a control strategy. The optimal manoeuvre, given an initial velocity, could be traded versus the aggressiveness of the braking using the results presented in this paper as a basis. Using a strategy with less severe braking in the cases where there is margin in the tyre-friction utilisation, could reduce the risk of inducing accidents with rear vehicles caused by heavy braking. Another reason to use a strategy with less severe braking is to intervene early rather than late, leaving room for a safety margin, without immediately resorting to heavy braking. Finally, in the double lane-change scenario, maximising the final velocity is related to the equivalent minimum-time manoeuvre, which can be preferable when there is opposing traffic. Specifically, it is therefore interesting how different braking strategies perform when varying the complexity of the scenario, and whether there exist any invariant strategies that can be used for all of the examined scenarios and thus control design.

## 2. Modeling

The vehicle model is based on the double-track chassis configuration illustrated in Figure 1. For a full description of the model equations and the parameters used, the reader is referred to the model referred to as DT WF in [13], which is the same model as the one used in this paper. Briefly, both longitudinal and lateral load transfer are included according to [14]. The centre of gravity of the vehicle body is suspended by a pendulum attached to the ground plane marking the vehicle position  $(X_p, Y_p)$ , with the suspension modelled as rotational spring-damper systems. A nonlinear tyre-force model is used, adopting the Pacejka's Magic Formula with weighting functions for modelling the tyre forces under combined longitudinal and lateral wheel slip [15]. As a particular feature, wheel dynamics is included in the model and the wheel torques are therefore the inputs, instead of the longitudinal tyre forces (commonly used in the literature). The braking system is modelled as a first-order system with the commanded torque  $T_{u,i}$  and the applied braking torque  $T_i$  for each wheel  $i \in \{1, 2, 3, 4\}$ . To model the fact that it is not possible to instantaneously achieve a desired steering angle  $\delta$ , the steering rate  $\dot{\delta}$  is used as an input to the vehicle rather than the steering angle, also enabling the steering rate to be constrained. The complete model of the vehicle system, i.e. the integrated chassis and wheel dynamics, is described by 23 dynamic states  $x$

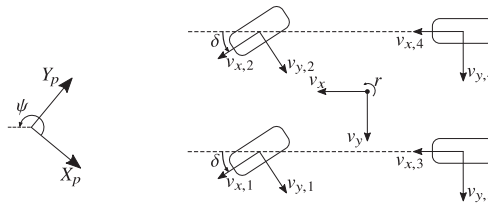


**Figure 1.** Double-track vehicle model.

**Table 1.** Vehicle states in the adopted double-track model with a nonlinear tyre-friction model.

Description	Notation
Position and orientation	$X_p, Y_p, \psi$
Velocity and yaw rate	$v_x, v_y, \gamma$
Roll and pitch motion	$\phi, \dot{\phi}, \theta, \dot{\theta}$
Steer angle	$\delta$
Applied wheel torques	$T_1, T_2, T_3, T_4$
Rotational wheel speeds	$\omega_1, \omega_2, \omega_3, \omega_4$
Wheel slip angles	$\alpha_1, \alpha_2, \alpha_3, \alpha_4$

and 5 inputs  $u$ . The inputs are the commanded torques  $T_{u,i}$  for each wheel  $i$  and the steering rate  $\dot{\delta}$ ; the states are defined in Table 1.

### 3. Scenarios

This section presents the manoeuvring scenarios considered in this paper. The first scenario is a left-hand turn, which is a both important and fundamental scenario that can be used to evaluate the effectiveness of stability-control systems in vehicles. The second scenario is a double lane-change, with geometry close to the ISO standard [16] used for testing of actual cars. The third scenario is an avoidance manoeuvre, which is to capture situations where the only objective is avoidance, e.g. when there are no lane limits or no opposing traffic.

#### 3.1. Left-hand turn scenario

The first scenario considered is a left-hand turn with constant curvature. Given that the origin of the vehicle position  $(X_p, Y_p)$  is in the centre of the circular turn, the deviation from the centre line of the road lane and the lane constraint are expressed as

$$e = \sqrt{X_p^2 + Y_p^2} - R, \quad |e| \leq d, \tag{1}$$

where  $R = 30$  m is the radius of the turn, and  $d = 1$  m is the lateral manoeuvring limit on the vehicle position  $(X_p, Y_p)$ . The vehicle is considered to have completed the manoeuvre at the time  $t_f$  when  $\dot{e}(t_f) \leq 0$ . This terminal condition represents that the vehicle will remain within the lane boundaries. In a specific manoeuvring case, this assumption can be verified by constructing continued trajectories such that  $\dot{e}(t) \leq 0 \forall t \geq t_f$ .

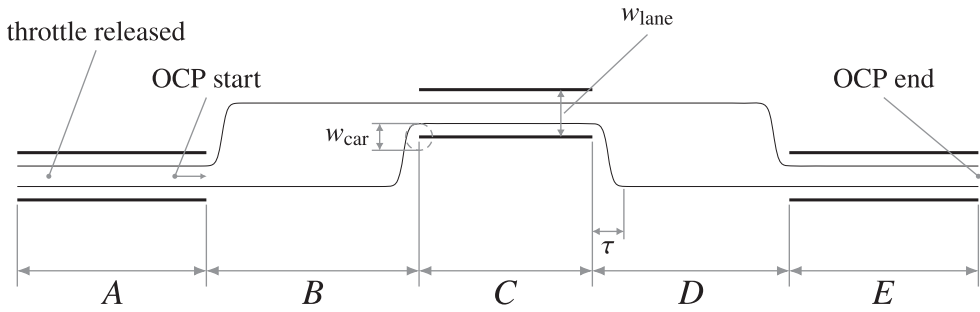


**Figure 2.** Double lane-change track. The black bars mark the placement of the cones in the ISO standard 3888-2 and the black curves mark the borders for the position  $(X_p, Y_p)$ .

### 3.2. Double lane-change scenario

The second scenario considered is the double lane-change shown in Figure 2, where the borders for the vehicle position  $(X_p, Y_p)$  are marked with black curves. The numerical parameters used for the track are collected in Table 2. The track is modelled by defining maximum and minimum limits on the position  $Y_p$ , for each value of the vehicle position  $X_p$ . This modelling introduces the following lane constraints in the optimisation:

$$\begin{aligned} Y_p &\leq a + c(H(X_p - X_{t1}) - H(X_p - X_{t2})), \\ Y_p &\geq -a + c(H(X_p - X_{b1}) - H(X_p - X_{b2})), \end{aligned} \quad (2)$$

where  $H$  denotes the Heaviside step function and  $a$ ,  $c$ ,  $X_{t1}$ ,  $X_{t2}$ ,  $X_{b1}$ , and  $X_{b2}$  are track parameters. The step function is, for numerical computational reasons in the optimisation, approximated as

$$H_{\text{sigmoid}}(x) = 0.5(1 + \tanh(2\pi x/\tau)), \quad (3)$$

where  $\tau$  is a parameter that determines the steepness of the step approximation. The track parameters are chosen based on the test defined in the ISO standard 3888-2 [16] for a severe lane-change obstacle-avoidance manoeuvre, with some simplifications such as making the lane width  $w_{\text{lane}}$  of all sections 3 m, whereas in the ISO standard the widths of the different sections are dependent on the vehicle width. In the ISO standard, the vehicle has to pass between cones without moving them. To approximate this situation, while keeping the parameterisation simple and only constraining the vehicle position  $(X_p, Y_p)$ , the size of the drivable area is made more narrow to account for the width of the vehicle,  $w_{\text{car}}$ . Note in Figure 2, that the approximate step function (3) contributes to the validity of this approximation. In the ISO standard, the throttle is released 2 m into the track. For the optimal control problem to be solved in this paper, the start point is arbitrarily set 10 m into the track. This choice is to limit the available initial braking distance, since vehicle systems typically tested on the track would not resort to full braking directly after the throttle is released. In summary, the double lane-change scenario represents an adaptation of the classical vehicle safety tests performed with new cars that still comprises the distinct characteristics of the ISO test, and the results are well suited for comparative studies.

**Table 2.** Parameters used for the double lane-change track. All of the parameter units are in metres.

Notation	Value [m]
$A$	12
$B$	13.5
$C$	11
$D$	12.5
$E$	12
$w_{\text{lane}}$	3
$w_{\text{car}}$	1.7
$\tau$	2
$a$	$(w_{\text{lane}} - w_{\text{car}})/2$
$c$	$w_{\text{lane}} + 1$
$X_{r1}$	$A + \tau/2$
$X_{r2}$	$A + B + C + D - \tau/2$
$X_{b1}$	$A + B - \tau/2$
$X_{b2}$	$A + B + C + \tau/2$

### 3.3. Avoidance-manoevre scenario

The track used for modelling the double lane-change scenario is also used to examine an avoidance-manoevre scenario. While the double lane-change takes place on the complete track with two obstacles, one in the right lane and one in the left lane, the avoidance-manoevre scenario only lasts until the initial obstacle has been avoided. Considering that a vehicle performing the avoidance-manoevre scenario does not have to take future obstacles into account, it should be possible to perform it with a higher velocity compared to the double lane-change scenario. It is interesting to study what implications future obstacles have on the driving strategy that should be employed. The avoidance scenario is similar to that of the left-hand turn, in that only a single turn is needed to complete the manoeuvre. It is therefore interesting to compare successful strategies in these scenarios, to investigate if one is also applicable to the other on a more general level.

## 4. Optimal control problem formulation

The analysis in this paper is based on a new optimisation criterion in an optimal control problem (OCP). The criterion (4a) is described in Section 1.2 and is the source of the key contributions in this paper. It is a linear combination of the initial velocity,  $v_0$ , and the final velocity  $v_f$ . The interpolation parameter  $\eta$  is limited to the interval  $0 \leq \eta \leq 1$ . The OCP includes constraints on the control inputs  $u$ , i.e. the wheel torques  $T_{u,i}$ , and the steering rate  $\dot{\delta}$ . Mathematically, the OCP is stated over the time interval  $[t_0, t_f]$  as follows:

$$\text{minimise} \quad -\eta v_0 - (1 - \eta)v_f \quad (4a)$$

$$\text{subject to} \quad T_{u,i,\min} \leq T_{u,i} \leq 0, \quad i \in \{1, 2, 3, 4\}, \quad (4b)$$

$$|\delta| \leq \delta_{\max}, \quad |\dot{\delta}| \leq \dot{\delta}_{\max}, \quad f(X_p, Y_p) \leq 0, \quad (4c)$$

$$F_c x(0) = \tilde{x}_0, \quad G_c x(t_f) = \tilde{x}_f, \quad g(x(t_f)) \leq 0, \quad (4d)$$

$$\dot{x} = G(x, z, u), \quad h(x, z, u) = 0, \quad (4e)$$

where  $f(X_p, Y_p)$  is the lane constraint for the vehicle position  $(X_p, Y_p)$  in the global coordinate system,  $F_c$  is a matrix with zeros and ones defining the states that have initial conditions,  $\tilde{x}_0$  is the corresponding initial condition,  $G_c$  is a matrix with zeros and ones defining the states where terminal equality constraints exist,  $\tilde{x}_f$  is the corresponding terminal equality constraint, and  $g(x(t_f))$  is the terminal inequality constraint. The chassis and tyre models are formulated as a semi-explicit differential-algebraic equation (DAE) system, defined by the functions  $G$  and  $h$ , where  $z$  denotes the algebraic variables. The chassis and tyre model are briefly described in Section 2; the dynamic and algebraic relations corresponding to  $G$  and  $h$ , together with vehicle parameters, are provided in [13]. The numerical values of the input constraints are  $\delta_{\max} = 0.5$  rad,  $\dot{\delta}_{\max} = 1$  rad/s, and  $T_{u,i,\min} = -\mu_{x,i}mgR_w$ , where  $\mu_{x,i}$  is the longitudinal friction coefficient of tyre  $i$ ,  $m$  is the vehicle mass,  $g$  is the gravitational acceleration constant, and  $R_w$  is the wheel radius. Among the initial states at time  $t=0$  of the manoeuvre,  $v_0$  is a free parameter; the manoeuvre is terminated once the desired final states defined by  $\tilde{x}_f$  are reached and  $g(x(t_f)) \leq 0$  is fulfilled.

## 5. Results

In this section, the approach for computing the solution to the OCP (4) is described. Moreover, solutions to the OCP for the considered vehicle manoeuvres are presented and analysed in detail, using the different measures for interpretation and evaluation defined in Section 5.1. Considering that the left-hand turn is a *de facto* standard manoeuvre for evaluating performance of vehicle handling, slightly more focus is put on this manoeuvre in the following analysis. General observations regarding the vehicle behaviour for different choices of the interpolation parameter  $\eta$  defined in (4a), and their implications for advanced active-safety systems and future autonomous cars, are provided in the subsequent Section 6.

Solving the OCP for the vehicle and chassis models, relies on the overall solution methodology developed and presented in [13]. Since analytical solutions of the continuous time OCP are intractable, direct collocation [17] was used to transform the problem into discrete optimisation variables, resulting in a large non-linear program (NLP) to be solved numerically. To this purpose, the optimisation framework JModelica.org [18] was used together with the NLP solver IPOPT [19] integrated with the linear solver HSL MA57 [20].

The OCP (4) is solved for a selected set of values of  $\eta$  for each scenario. Note that the selection of the values of  $\eta$ , for which the OCP solutions are presented, is different for the three scenarios considered. This is to ensure that each scenario exhibits a variety of braking behaviours. The initial guess in the iterative numerical optimisation was set to 50 km/h for  $v_0$  and 4 s for  $t_f$ . Except these values, no initialisation of the trajectories of the model variables was required to solve the OCP for the different scenarios considered. Because of numerical oscillations appearing in the steering angle and related quantities, a small weight on the steering rate is added by introducing the term  $10^{-4} \int_0^{t_f} \dot{\delta}(t)^2 dt$  in the optimisation criterion (4a) of the OCP. The leading constant is sufficiently small, such that the additional term does not influence any of the examined quantitative or qualitative measures of the manoeuvres, such as the initial and final velocity.



## 5.1. Additional interpretation and evaluation measures

In this section, quantities and measures are defined that are complementary to the model variables (see Table 1) and the value of the optimisation criterion (4a) in the analysis of the results. These measures provide additional insights later when analysing the computed optimal manoeuvres.

### 5.1.1. Force orthogonal to vehicle path

Given the longitudinal and lateral forces acting on the vehicle,  $F_x$  and  $F_y$ , respectively, and the body slip, defined as  $\beta = \arctan(v_y/v_x)$ , the force perpendicular to the vehicle path,  $F_{\perp}$ , is defined

$$F_{\perp} = F_y \cos(\beta) - F_x \sin(\beta). \quad (5)$$

This quantity is interesting since it, together with the velocity, is closely related to the current curvature of the vehicle path. By examining this variable, information about when the vehicle path curvature is limited by the available tyre forces is obtained.

### 5.1.2. Brake induced yaw-moment components

The yaw moment – i.e. the moment about the  $z$ -axis of the vehicle – is an important variable when analysing the yaw-control and lane-keeping control strategies. The contribution to the yaw moment from the applied braking force on each individual wheel is given by the contribution of the longitudinal force, together with the loss of lateral force because of longitudinal tyre slip [2]. For each wheel  $i \in \{1, 2, 3, 4\}$ , the expression for this contribution  $\Delta M_i$  is

$$\Delta M_i = \begin{bmatrix} l_{x,i} & l_{y,i} \end{bmatrix} \begin{bmatrix} F_{x,i} \sin(\delta_i) + (F_{y,i} - F_{y0,i}) \cos(\delta_i) \\ (F_{y,i} - F_{y0,i}) \sin(\delta_i) - F_{x,i} \cos(\delta_i) \end{bmatrix}, \quad (6)$$

where  $l_{x,i}$  and  $l_{y,i}$  are the longitudinal and lateral distances from the centre of rotation in the vehicle frame to wheel  $i$ , respectively,  $\delta_i$  is the difference in angle between the ego direction of wheel  $i$  and that of the vehicle,  $F_{x,i}$  and  $F_{y,i}$  are the longitudinal and lateral force acting on wheel  $i$ , respectively, and  $F_{y0,i}$  is the nominal lateral force on wheel  $i$  in the absence of braking forces.

As a means of distinguishing yaw-moment generation from braking to decrease the velocity, it is interesting to separate braking that causes a moment contribution in the counterclockwise direction from braking that causes a moment contribution in the opposite direction. For the vehicle model and the scenarios examined in this paper, braking of the left-hand side (LHS) wheels gives a moment contribution in the counterclockwise direction, and braking of the right-hand side (RHS) wheels gives a moment contribution in the clockwise direction. Note that owing to wheel inertia, some wheels can give a very small moment contribution in the opposite direction. It is also interesting to study the total contribution to the moment from the braking forces of all wheels. Thus, the braking-induced moments that are studied in the analysis of the manoeuvres are

$$\Delta M_{\text{left}} = \Delta M_1 + \Delta M_3, \quad \Delta M_{\text{right}} = \Delta M_2 + \Delta M_4, \quad \Delta M = \Delta M_{\text{left}} + \Delta M_{\text{right}}. \quad (7)$$

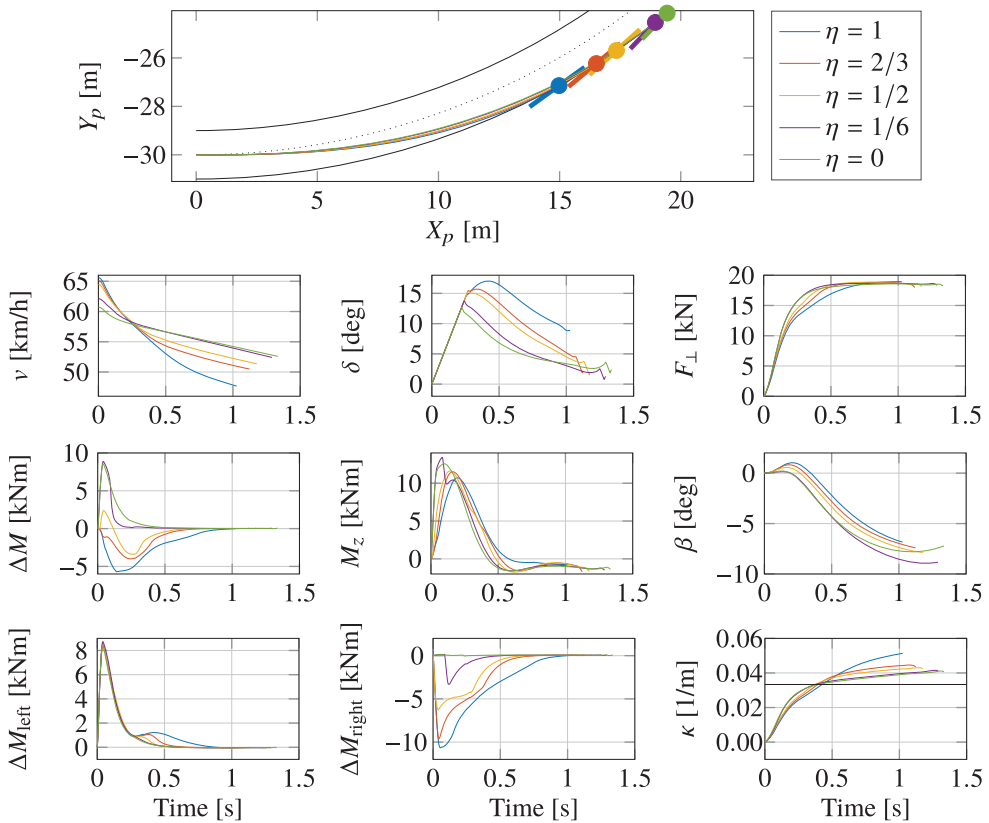


**Figure 3.** Optimal trajectories for different  $\eta$  when entering a turn with radius 30 m and width 2 m:  $v$ , vehicle velocity;  $\delta$ , steering angle;  $F_{\perp}$ , force perpendicular to vehicle path;  $\Delta M$ , brake-induced moment;  $M_z$ , total moment;  $\beta$ , body slip;  $\Delta M_{\text{left}}$ , brake-induced moment by the LHS wheels;  $\Delta M_{\text{right}}$ , brake-induced moment by the RHS wheels;  $\kappa$ , curvature of the vehicle path.

## 5.2. Left-hand turn

The left-hand turn is examined for an initial position at the centre of the lane at  $(X_p, Y_p) = (0, -30)$  m. Figure 3 illustrates solutions to the OCP, showing the vehicle path and selected vehicle trajectories for different values of  $\eta$ . In the upper plot, the geometry of the left-hand turn is illustrated together with the vehicle path in the respective case, where dots mark the final vehicle position with corresponding thick lines depicting the final vehicle orientation.

### 5.2.1. Left-hand turn: braking

The vehicle enters the turn at different velocities, depending on  $\eta$ . As can be observed in the differences in the velocity trajectories  $v$  for the computed optimal solutions in Figure 3, a higher initial velocity requires significantly more braking action during the manoeuvre. In the upper plot in Figure 3, it can be seen that with a higher initial velocity  $v_0$  (corresponding to a higher  $\eta$ ), the vehicle is faster drifting towards the outer boundary of the track. As a consequence, the required vehicle path to stay in the lane has a larger final (and maximum) curvature to compensate for the smaller curvature of the vehicle path in the beginning of the manoeuvre. Since the relative difference in curvature is hard to distinguish from the

vehicle paths, the curvature of the vehicle path  $\kappa$  is plotted in Figure 3, with the curvature of the centre line of the road marked as a black line. The difference in final velocity  $v_f$  in Figure 3 is limited by the available lateral tyre forces and the maximum curvature of the vehicle path. An effect that becomes apparent when applying more braking forces is that there are less lateral forces available, which can be seen in the plot of the force perpendicular to the vehicle path,  $F_{\perp}$ , in Figure 3. Towards the end of the manoeuvre, it can be seen that  $F_{\perp}$  is approximately the same for all  $\eta$ .

### 5.2.2. Left-hand turn: moment generation

In the plot of the steering angle  $\delta$  in Figure 3, it can be observed that the steering rate  $\dot{\delta}$  is in all cases saturated from the start of the manoeuvre until  $t \approx 0.25$  s, after which it decreases. This behaviour implies that additional turn-in moment most likely would be beneficial. However, as can be seen from the brake-induced moment  $\Delta M$  in Figure 3, resulting from the applied braking torques, the applied braking forces do not contribute to the turn-in moment for all values of  $\eta$ . Depending on  $\eta$  in the optimisation criterion (4a),  $\Delta M$  is either a turn-in moment, a turn-out moment, or its sign varies with time. Note that as expected, the total moment  $M_z$  in Figure 3 in all cases results in a turn-in yaw rate. The brake-induced yaw moment by the outer wheels,  $\Delta M_{\text{right}}$ , is heavily dependent on  $\eta$  as seen in Figure 3. For  $\eta = 1/6$ , there is a different strategy where the solution waits for the turn-in moment to build up before applying any braking torques on the outer wheels. For  $\eta = 0$ , similar to a traditional yaw-control strategy, no torque is applied on the outer wheels. The brake-induced turn-in yaw moment,  $\Delta M_{\text{left}}$ , can in Figure 3 be seen to be essentially independent of  $\eta$ ; the solutions differ only later in the manoeuvre when the vehicle starts to decrease the steering angle. The peak observed in the plot of  $\Delta M_{\text{left}}$  in Figure 3 is limited by the available friction forces of the tyres. The rise and sink times of the peak are primarily limited by the first-order dynamics between the commanded and the actual wheel torque. In Figure 3, it can be concluded from the negative sign of  $\beta$  when it is at its maximum absolute value, that additional turn-out moment for solutions obtained with higher  $\eta$  contributes to a lower body slip  $\beta$ .

### 5.2.3. Left-hand turn: tyre-force utilisation

Another interesting aspect to investigate is the tyre-force utilisation of each wheel, and how this utilisation relates to the value of the parameter  $\eta$  in the optimisation criterion. Figure 4 shows the tyre-force utilisation of each tyre for different  $\eta$  in the left-hand turn scenario. As suggested by [10], utilising both of the inner wheels is beneficial for yaw-control systems to improve their lane-keeping capability, which is clear also from Figure 4 since all strategies utilise both of the LHS wheels. It can be seen that the rear RHS wheel is utilised more than the front RHS wheel. This observation is explained by the fact that longitudinal and lateral tyre forces are coupled, and that longitudinal braking reduces the lateral tyre forces. For a left-hand turn, the reduction of the lateral tyre force from braking gives a contribution to the turn-in moment from the rear wheels, but a turn-out moment from braking the front wheels. Thus, relative to braking the front RHS wheel, braking the rear RHS wheel provides more turn-in yaw moment. It is interesting to note in Figure 4 that for the extreme case  $\eta = 1$ , all the individual tyre forces are close to the friction-ellipse limit. This observation means that braking is applied to always keep them close to this limit. The turn-out moment obtained from the braking torques for  $\eta = 1$ ,  $\Delta M$  in Figure 3, is thus the result

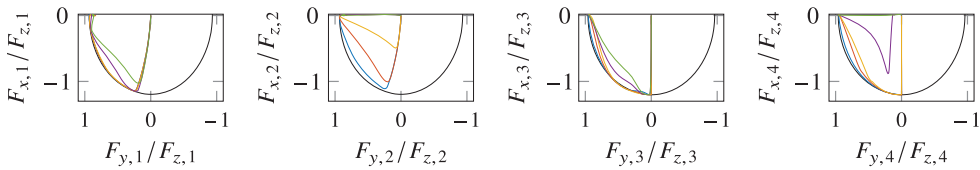


**Figure 4.** Resulting utilisation of the tyre forces for each wheel during the left-hand turn scenario for different  $\eta$ . The tyre forces are normalised with the normal force  $F_{z,i}$  of each wheel  $i$ . The black line marks the friction-ellipse limits. The legend is according to Figure 3.

from utilising all available tyre forces. In contrast, decreasing the interpolation parameter  $\eta$  leads to solutions in Figure 4 that are not close to the friction limit. For these solutions, it can be observed in Figure 3 that some degree of tyre-force utilisation is sacrificed for a larger turn-in moment,  $M_z$ , larger lateral forces,  $F_{\perp}$ , or less velocity reduction.

### 5.3. Double lane-change

The double lane-change scenario is examined for the parameters given in Table 2, with the initial position of the vehicle being  $(X_p, Y_p) = (10, 0)$  m, and the final position  $(X_p, Y_p) = (61, 0)$  m. Figure 5 illustrates the situation considered, with the vehicle path and selected optimal vehicle trajectories plotted for different values of  $\eta$ . In the upper plot, the vehicle paths for the respective value of the interpolation parameter are plotted in the double

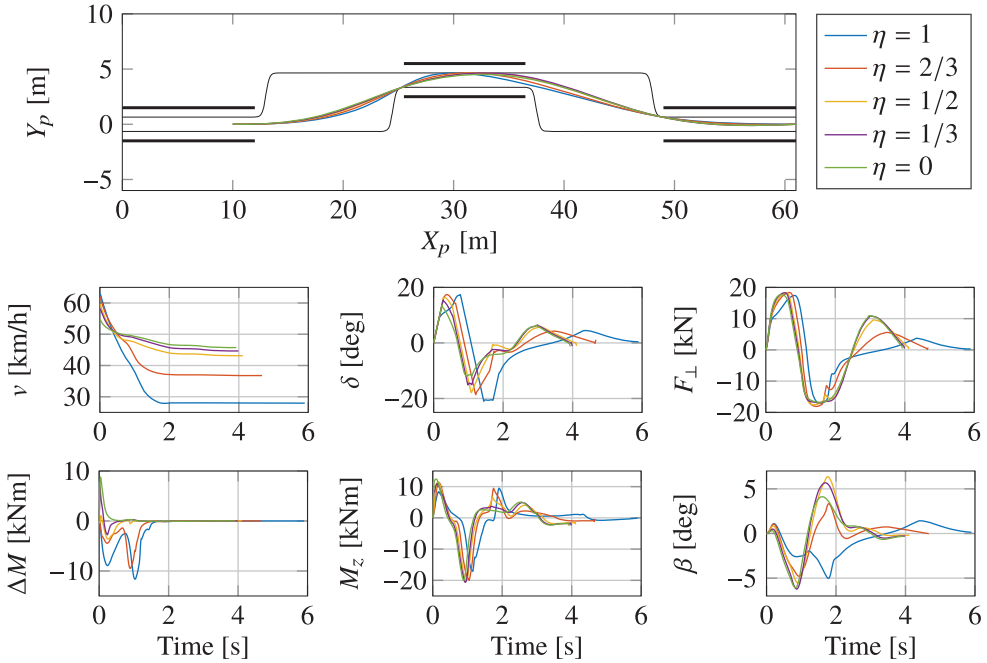


**Figure 5.** Optimal trajectories for different  $\eta$  when performing a double lane-change manoeuvre:  $v$ , vehicle velocity;  $\delta$ , steering angle;  $F_{\perp}$ , force perpendicular to vehicle path;  $\Delta M$ , brake-induced moment;  $M_z$ , total moment;  $\beta$ , body slip.

lane-change track (see Figure 2). The path for  $\eta = 0$  does not touch the upper boundary during the middle section of the track and is thus only limited by the lane constraint at  $X_p = 25.5$  m and 49 m. The body slip  $\beta$  is relatively small during the manoeuvre, reaching a maximum of approximately  $\pm 6$  degrees, meaning that the vehicle orientation is almost following the vehicle path. Analysing the velocity  $v$  and the perpendicular force  $F_{\perp}$  in Figure 5 closer, the final velocity seems restricted by the right-hand turn at around  $t \approx 1.5$ –2 s. At that time, the perpendicular force  $F_{\perp}$  is the limiting quantity, and for the remaining parts of the manoeuvre the decrease in velocity is minor. During the initial left turn, the body slip  $\beta$  is primarily negative. At the follow-up turn to the right,  $\beta$  is positive for all  $\eta$  except  $\eta = 1$ , but during that part the vehicle is driving comparably slow while turning fast. From the plot of the steering angle  $\delta$  in Figure 5, it is clear that the steering rate  $\dot{\delta}$  is saturated for a large part of the manoeuvre before  $t = 1.5$  s. During the first second of the manoeuvre, the brake-induced moments  $\Delta M$  are very similar to those in the left-hand turn in Figure 3. For the solutions obtained with  $\eta \geq 1/2$ , additional turn-in moment is generated during the right-hand turn by braking the RHS wheels of the vehicle, as can be seen in the plot of  $\Delta M$ .

#### 5.4. Avoidance manoeuvre

The avoidance-manoeuve scenario is examined in the same track as the double lane-change, using the track parameters given in Table 2. Also, the same initial position  $(X_p, Y_p) = (10, 0)$  m as in the double lane-change scenario is used, but the final position is chosen at the edge of the first obstacle at  $X_p = 25.5$  m, without any specified  $Y_p$  coordinate. The upper plot in Figure 6 illustrates the situation considered, with a subset of the track from Figure 2 and the resulting vehicle path for different values of  $\eta$ , where the corresponding thicker line depicts the final vehicle orientation. In addition, Figure 6 shows selected vehicle trajectories. Comparing the initial velocities with those achieved for the double lane-change scenario in Figure 5, the initial velocity  $v_0$  has increased 1.3% for  $\eta = 1$  and 8.6% for  $\eta = 0$ . Comparing the overall behaviour with the initial turn in the double lane-change scenario in Figure 5, and with the results for the left-hand turn in Figure 3, similarities are clear.

## 6. Discussion

In this section, implications of the braking behaviours observed in Section 5, resulting from the optimisation criterion (4a) are studied in light of the scenarios considered and some of the most related research, in order to find common behaviours useful for future control-system developments. With the perspective of future autonomous safety systems, several interesting common behaviours are observed for the manoeuvres in the different scenarios when studying the optimal solutions in detail. Such observations hold promise for the future practical applicability of the results presented, e.g. in lane-keeping control systems such as those presented in [9,11].

### 6.1. The family of braking patterns

In Section 5, time-critical manoeuvring situations were investigated. Analysing the results of computing optimal manoeuvres using the criterion (4a), it can be concluded from

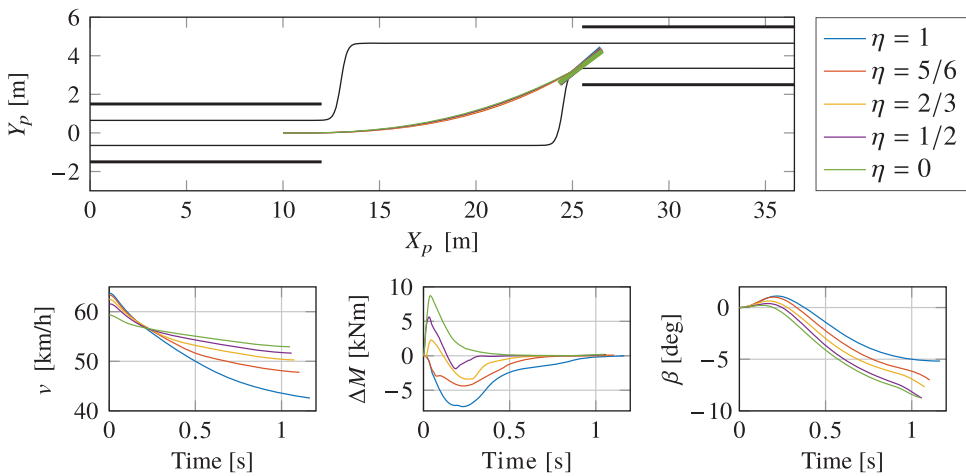


**Figure 6.** Optimal trajectories for different  $\eta$  when performing an avoidance manoeuvre:  $v$ , vehicle velocity;  $\Delta M$ , brake-induced moment;  $\beta$ , body slip.

Figures 3–6 that for  $\eta = 1$ , solutions close to a pure lane-keeping strategy are obtained – i.e. heavy braking on all wheels to reduce the velocity under consideration of the available tyre friction. Decreasing the interpolation parameter  $\eta$  in contrast leads to solutions closer to traditional yaw control, where the majority of the braking is applied on the inner wheels (see in particular Figure 3 with the results for the left-hand turn). For intermediate values of  $\eta$ , there are solutions where the initial turn-in moment is kept, and then changed to a turn-out moment later in the turn (see the plots of  $\Delta M$  in Figures 3, 5 and 6). This is similar to how an ESC acting on reference values for yaw rate and body slip performs in the same scenario, with the difference that in this paper these solutions have optimal braking with wheels on both sides of the vehicle at the same time. The investigated OCP formulation (4) consequently provides an approach for analysing and understanding the relation between traditional yaw control and optimal lane keeping for autonomous vehicles, since it embeds these strategies as the end-point values of the continuous interpolation parameter  $\eta$ , and gives a family of combined braking and steering behaviours in between.

## 6.2. Body slip

In [2], the body slip during optimal left-hand turn manoeuvres was reduced by introducing it as a weighted term in the objective function, while in [10] its absolute maximum was limited by introducing it as a constraint. The allowed body slip was in both papers concluded to have a small impact on the performance of all-wheel braking strategies for a single-turn scenario. However, on the contrary, the former paper in addition concluded that penalising high body slip has a significant impact on the performance of a yaw-control strategy where only the wheels on one side of the vehicle are allowed to brake. As observed in Section 5.2.2, to reduce the body slip  $\beta$  by using braking forces, it is desirable to produce a turn-out moment. Low- $\eta$  strategies, more similar to yaw control, mostly utilise braking for additional turn-in moment, which stand in conflict with reducing the body slip  $\beta$ . Additionally, a lower  $\beta$  requires more braking forces in order to utilise all of the available

tyre forces (see Figure 4). Consequently, all-wheel braking strategies with a lane-keeping approach have the additional benefit that they can reduce the experienced body slip during the manoeuvre, while still maintaining higher performance than traditional yaw control.

### 6.3. Different scenarios

When comparing Figures 3, 5 and 6, it can be observed that the characteristics between the left-hand turn, the initial turn of the double lane-change, and the avoidance manoeuvre are very similar. These observed common principles for actuation in different critical manoeuvre situations point forward towards practical realizations of lane-keeping control able to handle a multitude of scenarios with different complexity. When comparing the double lane-change to the avoidance manoeuvre, it is noted that the achieved initial velocity  $v_0$  is larger in the avoidance manoeuvre than the double lane-change. For the case  $\eta = 0$ , this difference is much larger than that for  $\eta = 1$ . This observation suggests that for this specific track, braking strategies computed for values of  $\eta$  close to one are more resilient to future lane constraints. One reason is the lower velocity achieved at the end of the first turn using a more braking-heavy strategy. Another reason is that, as discussed in Section 6.2, a high- $\eta$  strategy can more effectively control the body slip  $\beta$ . Considering  $\beta$  in the double lane-change in Figure 5, it can be seen that it is kept small during the initial turn, in particular for  $\eta = 1$ . Maintaining a low body slip is helpful when transitioning to turning in the opposite direction. When considering potentially complex scenarios involving more than turning in a single direction, it can thus be beneficial to not only lower the velocity, but also maintain a modest body slip. In the double lane-change manoeuvre, it can be concluded from the plot of  $F_{\perp}$  in Figure 5, that only the first two turns are critical since  $F_{\perp}$  is small in the following turn. This demonstrates that not adding energy to the system by the use of driving torques, implies that the complexity of the manoeuvre is limited by the initial velocity.

### 6.4. Different road conditions

It is of interest to investigate if the observed fundamental braking behaviours for different  $\eta$  change when the road conditions vary. To study this aspect, the friction coefficients (corresponding to dry asphalt) in the tyre-force model were scaled to 50% of their original values. A subset of the resulting trajectories are shown in Figure 7, and the results show that the characteristics in terms of the trade-off between yaw control and all-wheel braking observed on the high-friction surface still hold true. The results in Figure 7 indicate that the fundamental braking behaviours observed for different  $\eta$  are consistent for varying road conditions. Additionally, the same consistent behaviour has been observed for other optimal trajectories for both the left-hand turn scenario and the double lane-change scenario (not shown here to save space), with the friction coefficients scaled down to 30% of their original values. These are important observations, showing that the fundamental behaviours of the braking and steering patterns observed for the different scenarios in the results are the same for a wide range of surface conditions, including high-slip surfaces such as snow or ice (see also [4] for an analysis of optimal manoeuvre on different surfaces).

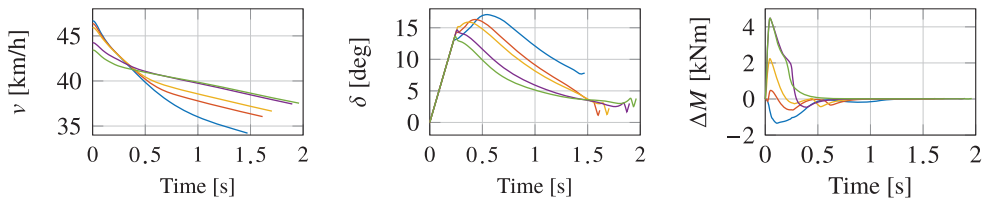


**Figure 7.** Optimal trajectories for different  $\eta$  when entering a turn with radius 30 m and width 2 m under low-friction conditions (50% of the nominal values):  $v$ , vehicle velocity;  $\delta$ , steering angle;  $\Delta M$ , brake-induced moment. The legend is according to Figure 3.

## 6.5. Devising control strategies

From a practical control perspective, it is interesting to investigate how the results obtained in this paper can be used for autonomous control in a car, both for comparative studies and for devising new strategies. An example of using results from this paper to design a controller can be found in [21], where the fact that the tyre forces for  $\eta = 1$  are close to the friction limit of the tyres was exploited to develop a controller for combined braking and steering. Of the many possibilities to utilise the results presented in Section 5, the following is another example.

### 6.5.1. Control based on constant front-wheel slip angle

In Figure 4, it can be seen that all tyres eventually reach close to maximum lateral tyre force. Further, the steering angle is initially rapidly increased in all scenarios. These observations are similar to the behaviour found for a professional race-car driver in [22]. There, it was found effective to keep the slip angle of the front wheels at the peak of lateral tyre friction during minimum-time cornering manoeuvre. Combining these observations motivates a strategy controlling the front-wheel slip angle  $\alpha_f$  (being the lumped slip value of the two front wheels) towards a reference  $\alpha_{f,\text{ref}}$  (close to the peak of lateral tyre friction) in combination with a braking pattern. To this end, the steering rate is not an optimisation variable and is instead given by the following control law:

$$\alpha_f = \delta - \arctan\left(\frac{v_y + rl_f}{v_x}\right), \quad \dot{\delta} = -\frac{\dot{\delta}_{\text{max}}}{\pi/2} \arctan\left(\frac{\alpha_f - \alpha_{f,\text{ref}}}{\varepsilon}\right), \quad (8)$$

where  $l_f$  is the distance to the front axle and  $\varepsilon$  is a tuning parameter. Using the reference  $\alpha_{f,\text{ref}} = 0.2$  rad and  $\varepsilon = 10^{-3}$ , an optimisation was carried out for the left-hand turn scenario for different values of  $\eta$ ; the results are shown in Figure 8. Interesting enough, the braking patterns retain the same characteristic behaviour as when the steering angle was a free optimisation variable. To see this, compare the striking similarity for  $\Delta M$  in Figure 3 and Figure 8. Further, for  $\eta = 1$ , the achieved initial velocity using the control law (8) is 99.9% of the initial velocity achieved when the steering angle is a free optimisation variable. This comparison with the optimal solution proves that a constant slip-angle strategy can be very effective in safety-critical manoeuvres and works well in tandem with the braking strategies encompassed by the family of braking patterns obtained by variation of the interpolation parameter  $\eta$ . It also gives insight into race driving.



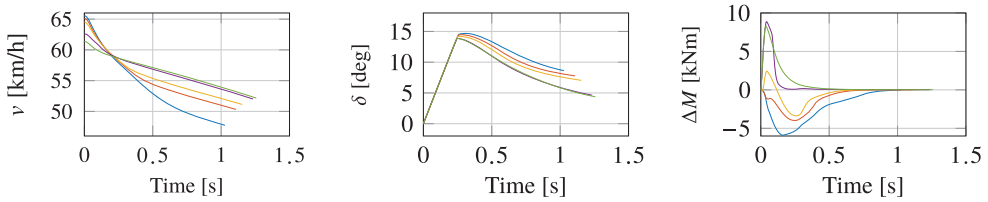


**Figure 8.** Optimal trajectories for different  $\eta$  when entering a turn with radius 30 m and width 2 m using the steering-rate input according to (8):  $v$ , vehicle velocity;  $\delta$ , steering angle;  $\Delta M$ , brake-induced moment. The legend is the same as in Figure 3.

### 6.5.2. Braking strategy

Continuing from the previously discussed constant front-wheel slip-angle steering strategy, it is desirable to achieve close to maximum lateral tyre force also on the rear wheels. This is important to make the force  $F_{\perp}$  perpendicular to the vehicle path larger, and thus increase the curvature of the vehicle path. With a constant slip-angle steering strategy as in the previous paragraph, additional yaw-moment control has to be taken care of by braking and traded against braking all four wheels to reduce the velocity. Giving priority to yaw moment and reaching large  $F_{\perp}$  faster can be important if the velocity is not very large (given the path curvature), but the road margins are small, or if it is a situation as in the follow-up turn in the double lane-change manoeuvre where there is a turn with large curvature after exiting a turn in the opposite direction (see Figure 5). If the required yaw moment is small, a braking strategy involving heavy braking of all four wheels can be used (see, e.g. [21]). If the required turn-in yaw moment is large, the braking force applied to the outer wheels can be reduced according to the pattern observed in Figure 4, first reducing the braking on the outer front wheel, thereafter that of the outer rear wheel. As clear from Figures 3, 5 and 6, the additional brake-induced turn-in yaw moment should be applied as early as possible, while a turn-out moment is still relatively easy to achieve later in the turn owing to load transfer. It is therefore not unreasonable to consider a trade-off and simplification in the control strategy when it is expected that additional turn-in moment is needed. There, the outer front wheel is not used for braking to ensure a large initial turn-in moment, even though this is the tyre experiencing the highest normal force when turning and braking.

## 7. Conclusions

By formulating an optimisation criterion depending on the single interpolation parameter  $\eta$ , a family of steering and braking patterns has been obtained and examined. The criterion is based on intuition around entry velocity and exit velocity, and a main result is that it is shown that the two different strategies of optimal lane-keeping control and optimal yaw control are embedded in the formulation and result from the boundary values of  $\eta$ . Heavy braking of the inner wheels at the start of the manoeuvre is observed for all  $\eta$ , while the most notable difference when increasing  $\eta$  is an increase in braking of the outer wheels. The braking and steering behaviours for different  $\eta$  remain consistent over different scenarios and different road conditions, suggesting that a single control framework could handle a multitude of situations. For manoeuvres involving more than a single turn, the results indicate that it is not only beneficial to reduce the velocity, but also to maintain a modest

body slip. As a specific control strategy, maintaining a constant front-wheel slip angle was shown to be very effective to accomplish close to optimal steering behaviour for different  $\eta$ . Further, as demonstrated in Section 6.5.1, the optimisation criterion can be used to benchmark how close new strategies is to the optimal for different degrees of four-wheel braking. Overall, the results provide new insights and have the potential to be used for future safety systems that can seamlessly adapt the level of braking depending on the situation at hand.

## Disclosure statement

No potential conflict of interest was reported by the authors.

## Funding

The authors are members of the ELLIIT Excellence Center, the Strategic Area for ICT research, supported by the Swedish Government (Sveriges Regering). This research was partially supported by the Wallenberg AI, Autonomous Systems and Software Program (WASP) (Knut och Alice Wallenbergs Stiftelse), funded by the Knut and Alice Wallenberg Foundation.

## ORCID

Victor Fors  <http://orcid.org/0000-0003-4034-2868>

Björn Olofsson  <http://orcid.org/0000-0003-1320-032X>

## References

- [1] Rajamani R. Vehicle dynamics and control. 2nd ed. New York, United States: Springer; 2012.
- [2] Lundahl K, Olofsson B, Berntorp K, et al. Towards lane-keeping electronic stability control for road-vehicles. In: Proc. 19th IFAC World Congress. Cape Town, South Africa; 2014. p. 6319–6325.
- [3] Sundström P, Jonasson M, Andreasson J, et al. Path and control signal optimisation for over-actuated vehicles in two safety-critical maneuvers. In: 10th Int. Symp. Advanced Vehicle Control (AVEC10). Loughborough, United Kingdom; 2010.
- [4] Olofsson B, Lundahl K, Berntorp K, et al. An investigation of optimal vehicle maneuvers for different road conditions. In: 7th IFAC Symposium on Advances in Automotive Control (AAC). Tokyo, Japan; 2013.
- [5] Smith EN, Velenis E, Tavernini D, et al. Effect of handling characteristics on minimum time cornering with torque vectoring. *Vehicle Syst Dyn.* 2018;56(2):221–248.
- [6] Velenis E, Tsiotras P. Minimum time vs. maximum exit velocity path optimization during cornering. In: Proc. IEEE Int. Symp. on Industrial Electronics (ISIE). Dubrovnik, Croatia; 2005. p. 355–360.
- [7] Yang D, Gordon TJ, Jacobson B, et al. Optimized brake-based control of path lateral deviation for mitigation of secondary collisions. *Proc Inst Mech Eng Part D.* 2011;225(12):1587–1604.
- [8] Yang D, Gordon TJ, Jacobson B, et al. Quasi-linear optimal path controller applied to post impact vehicle dynamics. *IEEE Trans Intell Transp Syst.* 2012 Dec;13(4):1586–1598.
- [9] Ali M, Falcone P, Olsson C, et al. Predictive prevention of loss of vehicle control for roadway departure avoidance. *IEEE Trans Intell Transp Syst.* 2013;14:56–68.
- [10] Klomp M, Lidberg M, Gordon TJ. On optimal recovery from terminal understeer. *Proc Inst Mech Eng Part D.* 2014;228(4):412–425.
- [11] Gao Y, Gordon TJ, Lidberg M, et al. An autonomous safety system for road departure prevention based on combined path and sideslip control. In: The Dynamics of Vehicles on Roads and Tracks – Proc. 24th Symp. International Association for Vehicle System Dynamics (IAVSD2015); Graz, Austria. 2016. p. 281–286.

- [12] Fors V, Olofsson B, Nielsen L. Formulation and interpretation of optimal braking patterns in autonomous lane-keeping maneuvers. In: 2nd IAVSD Workshop on Dynamics of Road Vehicles. Berlin, Germany; 2017.
- [13] Berntorp K, Olofsson B, Lundahl K, et al. Models and methodology for optimal trajectory generation in safety-critical road-vehicle manoeuvres. *Vehicle Syst Dyn.* 2014;52(10):1304–1332.
- [14] Berntorp K. Derivation of a six degrees-of-freedom ground-vehicle model for automotive applications. Sweden: Department of Automatic Control, Lund University; 2013. (Technical Report; 7627).
- [15] Pacejka HB. Tyre and vehicle dynamics. 2nd ed. Oxford, United Kingdom: Butterworth-Heinemann; 2006.
- [16] ISO 3888-2:2011. Passenger cars – test track for a severe lane-change manoeuvre – part 2: obstacle avoidance. 2011.
- [17] Biegler LT, Cervantes AM, Wächter A. Advances in simultaneous strategies for dynamic process optimization. *Chem Eng Sci.* 2002;57:575–593.
- [18] Åkesson J, Årzén KE, Gäfvert M, et al. Modeling and optimization with Optimica and JModelica.org—Languages and tools for solving large-scale dynamic optimization problems. *Comput Chem Eng.* 2010;34(11):1737–1749.
- [19] Wächter A, Biegler LT. On the implementation of an interior-point filter line-search algorithm for large-scale nonlinear programming. *Math Program.* 2006;106(1):25–57.
- [20] HSL. A collection of Fortran codes for large scale scientific computation. 2017; Accessed: 2017 Feb 15; Available from: <http://www.hsl.rl.ac.uk/>
- [21] Fors V, Olofsson B, Nielsen L. Slip-angle feedback control for autonomous safety-critical maneuvers at-the-limit of friction. In: 14th Int. Symp. Advanced Vehicle Control (AVEC18). Beijing, China; 2018.
- [22] Laurence VA, Goh JY, Gerdes JC. Path-tracking for autonomous vehicles at the limit of friction. In: American Control Conference (ACC); Seattle, WA. 2017. p. 5586–5591.